Time-Resolved Dynamics of the Vesicle Membrane During Individual Exocytotic Secretion Events, as Extracted from Amperometric Monitoring of Adrenaline Exocytosis from Chromaffin Cells

Christian Amatore,* Yann Bouret, and Laurent Midrier

Abstract: In chromaffin cells, adrenaline is known to be released through docking and then fusion of a secretory vesicle to the cytoplasmic membrane of the cell. Here we propose a method for the calculation of the dynamics of the vesicle membrane during the fusion from amperometric currents observed during individual exocytotic secretion events. The method is based on recognition of the fact that the overall current spike shape results from the convolution of the membrane dynamics with the rate of diffusion and exchange of the catecholamine cation inside the matrix core of the vesicle. This convolution can be treated analytically thanks to a reasonable approximation on the relative time scales of the opening function and diffusion; this leads to a convolution integral with which one deconvolutes the experimental amperometric data. An alternative numerical treatment through Brownian motion simulations dispenses with the need for this simplifying approximation. Combination of both approaches yields the membrane dynamics with a precision and a time resolution never achieved before. The peculiar dynamics of the vesicle membrane hint that exocytotic events are regulated by the swelling of the matrix polyelectrolyte core of the vesicle (although this important component is transparent in the analysis proposed here); this points to the important role of matrix swelling in exocytotic behavior. In particular, the effect may be elaborated to offer a new energetic interpretation of the transition between pore release and fusion release: secretory vesicles which involve pores and matrices similar to those of the adrenal cells investigated here can be separated into two classes according to their radius and catecholamine content. Small vesicles ($<$ ca. 25 nm radius, and containing $<$ ca. 20000 molecules) should always release their contents through pore docking; larger vesicles should always fuse, unless another mechanism closes the pore before ca. 20000 molecules of catecholamine have been released.

Keywords: amperometry · exocytosis · neurotransmitters · secretory release · vesicles

Introduction

Regulated exocytosis of neurotransmitters commands the communication between neurons. As in neurons, in chromaffin and beige mouse mast cells which are current biological models for the investigation of neuronal exocytosis, the cationic catecholamine neurotransmitter is encapsulated in secretory vesicles present in the cytoplasm of the cell; it is contained in a polyelectrolyte gel matrix which fills the inside of the vesicle.[1, 2] Investigations of exocytotic events on chromaffin and mast cells through patch-clamp techniques have established that following stimulation of the cell by calcium ions,[3] the intracellular secretory vesicles dock with the membrane of the cell and connect to the extracellular medium via a pore that passes through the two membranes in contact. This creates a nanometric channel whose diameter remains constant during release, since it is imposed by the pore architecture.[4] This pore allows the release of the cationic catecholamine neurotransmitter into the extracellular fluid [4, 5] and therefore also provokes the simultaneous entrance of hydrated cations into the vesicle matrix, a process necessary to maintain electroneutrality within the vesicle matrix.

The release of biologically important molecules by cells can be monitored by cyclic voltammetry or amperometry at carbon-fiber ultramicroelectrodes.[4b, h, 5, 6] Amperometric monitoring of exocytotic events at chromaffin cells shows that in 20–30% of the events[5c] a constant flux of neurotransmitter is released at the beginning of the exocytosis, presumably through the initial pore. Indeed, this phenomenon can be rationalized on the basis of the analogy with steady-state spherical diffusion at ultramicroelectrodes. The radius (5 ± 1 Å) of the pore determined through this electrochemical analogy[5c] matched extremely closely that derived from

[a] Dr. C. Amatore, Y. Bouret, L. Midrier
Ecole Normale Supérieure
Département de Chimie, UMR CNRS 8640 PASTEUR
24, rue Lhomond, F-75231 Paris Cedex 05 (France)
Fax: (+33) 1-4432-3863
E-mail: amatore@ens.fr

 © WILEY-VCH Verlag GmbH, D-69451 Weinheim, 1999 0947-6539/99/0507-2151 $ 17.50+.50/0

patch-clamp measurements,[1–4, 7] although the two techniques are totally independent: patch-clamp sees the pore presence through modification of the capacitance of the patched membrane area, but is blind to the flux of catecholamines through this pore; conversely, amperometry is blind to the pore opening but sees the flux of neurotransmitter that ensues. Patch-clamp measurements indicate that the initial pore may close again; this observation is rationalized as the undocking of the vesicle from the cell membrane. Generally such events (docking/undocking) are not easily recognized on amperometric monitoring traces when they occur alone. However, when a pore release is observed in amperometry (~20–30% of the events), a few milliseconds after the initial opening of the pore one observes a sharp increase of the current (see sketch in Figure 1), followed by a smoother

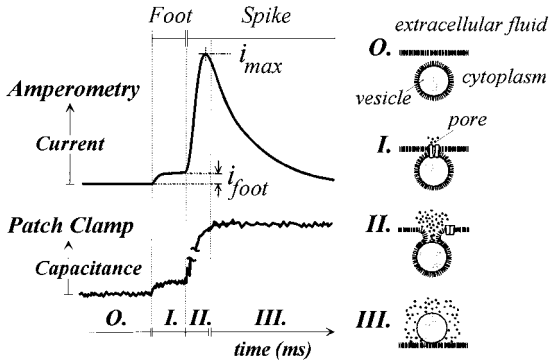

Figure 1. Schematic representation of an individual exocytotic secretion event monitored by patch amperometry, adapted from an original figure published in ref. [4h]. The current response (pA scale) as a function of time (top left) indicates the two components (foot and spike, see text) of the response of a chromaffin cell stimulated by Ca^{2+}, and is shown in parallel with the change of the patched area capacitance (bottom left) measured (fF scale) simultaneously by patch-clamp. On the right-hand side are sketched the four stages of the exocytotic event during each of the four domains labeled 0 to III on the left-hand side of the figure (note that the various components are not depicted to scale).

decrease of the flux, so that the main amperometric signal (termed the spike) is shaped as an exponentially modified gaussian[5c] that follows the smaller constant current plateau (termed the foot) which corresponded to the release by the pore. In most amperometrically detected events (~70–80%) only the spike component is observed, which can be explained by assuming that in most cases the duration of the pore is in the range of a millisecond or less, so that it is merged with the sharp rising part of the spike and cannot be resolved in the digitization process (e.g., 1 to 0.5 ms time increments; see Experimental Section for the experimental current traces). Since for ~20–30% of the events, the pore current is observable and has a mean duration of ca. 8 ms, a mean duration of ca. 2 ms appears a reasonable estimate when considering the whole set of events.[5d] Voltammetric measurements have established that the catecholamine released during the foot and during the spike is the same,[5b] namely, adrenaline for chromaffin cells. Therefore, the specific shapes of the foot and of the spike represent *directly and only* the time variations of the released flux.

Coupling of patch-clamp and amperometric techniques [4h] has established that the sharp rising branch of the spike corresponds to a sudden increase of the capacitance of the patched cell membrane area (see sketch in Figure 1). This feature is explained as a rapid increase of the patched surface area due to the incorporation of the vesicle membrane into the cell membrane by rapid fusion of the two bilipidic layers. Fusion implies a concomitant unmasking of the vesicle matrix wall, so that the matrix external surface becomes directly exposed to the extracellular medium and a larger amount of neurotransmitter can be released much more rapidly than by the pore. This increased release flux is reflected by the steep increase of the amperometric current. During the comparatively smoother current decay that follows this sudden rise, patch-clamp measurements indicate that there is no variation of the membrane area.[4h] One may therefore reasonably assume that the matrix external surface is then fully exposed to the extracellular solution at this stage, so that the smooth decrease of the amperometric current features mainly the slower and slower extraction of the neurotransmitter from the matrix core.

In summary, the particular shapes of the current spike and of the foot are thought to reflect the occurrence of three fundamentally distinct physicochemical processes that are schematized in Figure 1: pore creation, fusion and unwrapping of the vesicle membrane, and release of neurotransmitter from the fully exposed polyelectrolyte matrix, the two latter processes being certainly intimately coupled in producing the characteristic spike shape. When observable, the amount of neurotransmitter released during the foot is generally negligible (less than ~1%)[5c] compared with that released during the spike, as shown by the relative charges obtained by time integration of each currents. Thus, in a first approximation the pore phenomena (foot) can be disconnected from the fusion-initiated ones (spike) because the foot release is not expected to alter significantly the whole vesicle bulk (but see below in Section C of Results and Discussion). Conversely, the two physicochemical processes leading to the spike characteristic shape are expected to be intimately coupled. In a previous work,[5c] these two processes have been uncoupled empirically, the two components of the spike being arbitrarily (but vide infra) deconvoluted through fitting to an exponentially modified gaussian kinetics. Although this choice led to an excellent fit between experimental and reconstructed spikes, and afforded a first handle on the physicochemical parameters that govern the two distinct process, it was not fully satisfactory because based upon an arbitrary (albeit reasonable, vide infra) model.

In the present work, we wish to present a more physicochemical descriptive model of the spike events for secretion from vesicles that contain polyelectrolyte matrixes similar to those of adrenal cells which are considered in this work. We illustrate how this model can be used for routine extraction from any amperometric spike of the physicochemical parameters that characterize the vesicle and its matrix, but most of all how it permits the reconstruction of the opening function of the vesicle, that is, the variation over time of the vesicle surface area exposed to the extracellular fluid. This yields a much better definition than could be achieved up till now by

 © WILEY-VCH Verlag GmbH, D-69451 Weinheim, 1999 0947-6539/99/0507-2152 $ 17.50+.50/0 *Chem. Eur. J.* **1999**, *5*, No. 7

patch-clamp measurements based on the data reported in the current literature.[4h] On the basis of this much better definition, important conclusions can be inferred which should be valid for most cells containing polyelectrolyte matrixes similar to those of adrenal cells.

Results and Discussion

A. Theory

I. General framework of the model: In the amperometric experiments, a carbon-fiber microelectrode of micrometric size is positioned at the contact of the cell membrane so that diffusion of the adrenaline cations released from any vesicle (radius $R_0 \sim 150$ nm) fusing under the electrode surface is extremely fast compared with the half-width of the spikes (i.e., $t_{diff} \ll t_{1/2}$, with $5\ ms \leq t_{1/2} \leq 50-60$ ms, vide infra) and the collection efficiency of the electrode is unity for any event which occurs under its surface.[5c, 8] Thus, the current spike (Figure 1) monitored at the electrode through the two-electron oxidation of the adrenaline[9] at the electrode surface [Eq. (1)] reflects directly the flux of release without significant filtering by diffusion of adrenaline into the small extracellular fluid gap.[8] Because of the analogy with a real synapse, such electrochemical systems have been termed articifial synapses.[6a]

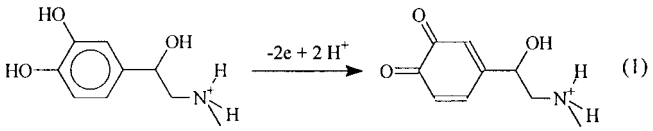

(1)

In addition to the two physicochemical factors that have been identified above in controlling the current spike shape—namely, i) the unfolding of the membrane, since this controls the rate of exposure of the surface area of the gel matrix which is initially encapsulated by the vesicle membrane; ii) the diffusion of the neurotransmitter from the inside core of the matrix towards the external surface area exposed to the solution—a third one needs also to be considered and relates to the swelling of the gel matrix[10] during the release due to its hydration and to the exchange of cations.

This third phenomenon may need some explanation. Indeed, when the matrix is in its initial packed form,[1] the protonated catecholamine cation is trapped in a compacted polyelectrolyte matrix whose anionic counterpart in chromaffin vesicles is formed by chromogranin A, a polyanion consisting of a peptidic backbone bearing a series of carboxylate groups that compensate the adrenaline cation electrostatic charges and are also expected to participate in numerous H-bonding and dipole–dipole interactions with the adrenaline cation. Thus the polyelectrolyte matrix inside the intact vesicle is tightly compacted[11] and the adrenaline cation is not expected to be able to diffuse with a rate compatible with the intensity of the current spike (viz., $D_{packed} \ll 10^{-12}\ cm^2 s^{-1}$). However, as soon as the gel matrix is exposed to the extracellular solution, its hydration and the cation exchange with the monovalent ions present in the extracellular medium are expected to make the polyelectrolyte matrix swell. This is well known for synthetic polyelectrolytes[11] and has also been observed visually in giant vesicles isolated from mast cells in which the matrix swells two to three times in volume (i.e., ca. 30–40% in radius).[12] Such swelling[13] is expected to disrupt the cohesion of the matrix and thus to loosen the interactions between the adrenaline cation and the polyanionic backbone of the matrix,[11] thus resulting in a drastic increase of the diffusion coefficient of the cations in the swollen parts.[11a, 12b]

From the above paragraph it follows that swelling and diffusion are necessarily intimately coupled, a fact that is fully documented in gel-swelling kinetic investigations. The matrix cannot swell locally before diffusion brings an adequate amount of monovalent ions. Conversely, diffusion of the adrenaline cation and its replacement by monovalent ions for electroneutrality cannot occur before swelling of the matrix allows a significant diffusion coefficient to be achieved locally. Since a precise experimental investigation of the dynamics of the gel at hand is presently out of reach for the case of chromaffin cell vesicles, for our present goal it is sufficient to decide if one of the two phenomena (diffusion or swelling) is controlling kinetically the overall mixed phenomena.

This important question has already been answered in a previous work.[5c] Postulating pure diffusion control (i.e., assuming an extremely fast local swelling, $t_{swell} = R^2 f/E \ll t_{1/2} \sim t_0 = R^2/D$, where f is the coefficient of friction between the polyelectrolyte network comprising the gel and the gel fluid, E the longitudinal bulk modulus of the network and D the average diffusion coeficient of water, ions, and adrenaline cations in the swollen matrix) affords descending branches with the correct shapes compared with the experimental current spikes.[5c] The converse assumption, namely control by swelling kinetics (i.e., for $t_0 = R^2/D \ll t_{1/2} \sim t_{swell} = R^2 f/E$), affords descending branches incompatible with the experimentally observed ones.[5c] Thus, on the basis of this earlier result, the problem at hand can be greatly simplified for chromaffin vesicles, since at each point where diffusion occurs significantly the swelling kinetics can be considered as occurring infinitely fast compared with the rate of diffusion of ions in and out the matrix.[14]

Moreover, because of the requirement of electroneutrality, the global concentration of cations is constant. It is then sufficient to take into account diffusion of the adrenaline cation alone; this allows further simplification of the physicochemical formulation of the system. In other words, in any zone where a change of the neurotransmitter concentration needs to be evaluated (i.e., where its concentration differs from the initial one), the matrix can be considered in its swollen state and the diffusion coefficient of the adrenaline cation taken as that in the swollen matrix. Conversely, where diffusion does not affect the neurotransmitter concentration, the matrix is unswollen, and technically a different diffusion coefficient ($D_{packed} \ll D$) should be considered.[12b] However, since in these zones diffusion, by definition, has not yet altered the concentration of adrenaline, a change from D_{packed} to D is irrelevant because the flux from these unswollen zones is nil. Therefore, within the framework of the above assumption on relative kinetics of diffusion and swelling, it is equivalent to consider diffusion of adrenaline into a homoge-

neous, fully swollen spherical matrix, even if one should bear in mind that the real matrix cannot be immediately swollen and that its spherical shape cannot be maintained in the course of swelling since the partial masking by the membrane creates an assymmetry.

Finally, the microelectrode is in close vicinity with the cell membrane and its potential set on the oxidation wave of adrenaline. These features, especially considering that the diffusion coefficient of the adrenaline cation in the extracellular fluid ($D_{ext} = 6 \times 10^{-6}\ cm^2 s^{-1}$) ought to be much larger than that inside the swollen vesicle ($D \simeq 10^{-8} - 10^{-7}\ cm^2 s^{-1}$,[12b] vide infra), allow us to assume that the concentration of the adrenaline cation is maintained at zero on the matrix border exposed to the extracellular fluid.

This whole set of considerations permits us propose the simple model sketched in Figure 2. The vesicle matrix is represented by a spherical volume of radius R, the swollen

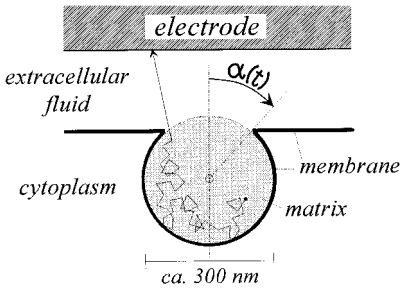

Figure 2. Model used in this work. The matrix is represented by the shadowed area and the fused cell and vesicle membranes by the solid thick curves. In addition the Brownian motion of a particle in the matrix is schematized along with its fast trapping by the electrode [Eq. (1)] as soon as it is released into the extracellular fluid.

radius ($R = \varepsilon R_0$, with $\varepsilon_{mean} \approx 1.35$ based on measurements on mast cells). Since the cell (ca. 10 μm radius) is considerably larger than the vesicle, the cell membrane is represented by an infinite plane which intersects the sphere so that an angle α is defined. This intersection delimits two zones on the matrix wall. On the part located under the cell membrane plane ($\alpha \leq \theta \leq \pi$) the vesicle membrane is intact so that this section of the vesicle wall remains impermeable to the adrenaline cation. Conversely, the former section of the vesicle membrane located above the plane ($0 \leq \theta \leq \alpha$) has been already incorporated into the cell membrane, so that this zone of the matrix is freely exposed to the extracellular medium. Its wall can be crossed by the adrenaline cation to reach the solution and its concentration is therefore maintained at zero on the wall due to its immediate electrochemical consumption. Within this framework, the evaluation of the current spike amounts to determine the variation over time of the flux ϕ of moles of adrenaline [viz., $i = 2F\phi$, where F is Faraday's constant; see Eq. (1)] crossing this opened wall when α varies as a function of time t.

To proceed further, a normalization of parameters and variables is necessary, because most geometrical and physicochemical properties of the system are a priori unknown for a given individual event, and are at best only known through mean estimates which cannot be used for analyzing one particular spike. This normalization is performed through the set of dimensionless variables defined in Equations (2) – (4),

$$\textit{time}: \quad \tau = Dt/R^2 = t/t_0 \tag{2}$$

$$\textit{space}: \quad \rho = r/R \tag{3}$$

$$\textit{number of moles}: \quad \eta = N/[(4/3)\pi R^3 (C_0/\varepsilon^3)] \tag{4}$$

where R is the radius of the swollen matrix, r the radial distance from the center of the spherical matrix, ε the coefficient of expansion of the matrix (viz., $\varepsilon = R/R_0$), C_0 the initial concentration of adrenaline inside the unswollen vesicle, and N the number of moles of adrenaline cation contained at time t inside the matrix (note that $N_0 = N_{t=0} = (4/3)\pi R^3 (C_0/\varepsilon^3)$ so that $\eta(\tau = 0) = 1$). With this set of dimensionless variables, the dimensionless instantaneous flux of adrenaline is given by Equation (5), where $t_0 = R^2/D$, and the

$$\textit{flux}: \quad \varphi(\tau) = d\eta/d\tau = \phi(t = t_0\tau) \times \{t_0/[(4/3)\pi(R/\varepsilon)^3 C_0\} \tag{5}$$

amperometric current at any time $t = \tau t_0 = \tau R^2/D$ is readily obtained from $\varphi(\tau)$ by means of Equation (6), so that solving

$$i(t) = [8\pi F D R C_0/(3\varepsilon^3)] \times \varphi(\tau = t/t_0) \tag{6}$$

the problem amounts to determining the dimensionless diffusion-controlled flux $\varphi(\tau)$ as a function of the dimensionless time τ, starting from the initial condition $\eta = 1$, $\alpha = 0$ at $\tau = 0$.

II. Uncoupling between rate of fusion of membranes and diffusion inside the matrix: The rate of fusion of the membranes, that is, the function $\alpha(t)$, controls the time variation of the matrix surface area exposed to the extracellular fluid, and therefore governs $\varphi(\tau)$. To the best of our knowledge and savoir-faire it is impossible to produce a general solution under such circumstances, especially since α(t) is unknown. However, on the basis of the results of patch-amperometric experiments (patch-clamp coupled with amperometry) we know that the variation of unwrapped surface area Σ(t) (i.e., of α) occurs within a time range which is much smaller than the actual half-width $t_{1/2}$ of the current spike (see Figure 1). This observation establishes that the rate of depletion by diffusion within the matrix core is much smaller than the rate of variation of the exposed surface area. Therefore, the coupling between fusion and diffusion can be treated at the level of a first-order filter approximation. In the Laplace plane (s is the Laplace variable corresponding to τ, and the Laplace transform of a function is indicated by underlining the real function) this means that the instant flux $\underline{\varphi}(s)$ is given by the direct product of the elementary flux per unit of surface area, $\underline{\Phi}(s)/4\pi$, where $\underline{\Phi}(s)$ would correspond to the flux of a completely unwrapped vesicle (i.e., for $\alpha = \pi\mathscr{H}(t)$, where $\mathscr{H}$ is the Heaviside unity step function) and is normalized to the total surface of the sphere [i.e., 4π in the dimensionless space, Eq. (3)], times $\underline{\vartheta}$(s), the Laplace transform of the elementary surface area resulting from a variation $d\alpha$ during the elementary time $d\tau$, namely, of $\vartheta(\tau) = d\Sigma/d\tau$.

© WILEY-VCH Verlag GmbH, D-69451 Weinheim, 1999
0947-6539/99/0507-2154 $ 17.50+.50/0 *Chem. Eur. J.* **1999**, *5*, No. 7

Thus we arrive at Equation (7), which shows that in the real time space, the flux is given by the convolution integral of

$$\underline{\varphi}(s) \simeq \underline{\Phi}(s)\underline{\vartheta}(s)/4\pi \tag{7}$$

Equations (8) and (9), $\sigma(\tau)$ being the fraction of the vesicle surface area that is exposed to the extracellular fluid at time $\tau = t/t_0 = Dt/R^2$.

$$\varphi(\tau) = \int_0^\tau \Phi(\tau - \zeta)\frac{\vartheta(\zeta)}{4\pi}\mathrm{d}\zeta \tag{8}$$

where

$$\int_0^\tau \frac{\vartheta(\zeta)}{4\pi}\mathrm{d}\zeta = \frac{\sum(\tau)}{4\pi} = 1/2\ [1 - \cos\alpha(\tau)] = \sigma(\tau) \tag{9}$$

The range of validity of the first-order approximation in Equation (8) has been checked by Brownian motion simulations and shown to be accurate provided that the spike presents a rising branch that is sharper than its descending branch, a prerequisite met by all experimental spikes. For these checks a series of arbitrary $\sigma(\tau)$ sigmoidal functions was generated and direct Brownian motion simulations were performed to generate a corresponding series of $\varphi(\tau)$ functions (see Appendix A). The choice of sigmoidal functions for the $\sigma(\tau)$ functions in these tests is justified by the patch-clamp observations (see Figure 1). From this series of $\varphi(\tau)$ functions, a series of $\sigma_{\mathrm{recov}}(\tau)$ functions was then recovered through numerical deconvolution of Equation (8) (see Appendix B) thanks to the independent knowledge of the function $\Phi(\tau)$ (see Figure 3, Eq. (10) and Appendix C).

$$\Psi(\tau) = \frac{3}{4}\left(\frac{1}{1 - \frac{1}{2}\mathrm{e}^{-1.12\left[0.52\times\tau^{0.56}\mathrm{e}^{-4.43\tau^{0.59}} + 1.11\times(\mathrm{e}^{-0.75\tau^{1.32}} + 1.18\tau - 1)\right]}} - 1\right) - 6.7\times10^{-3}\times\tau^{4.8\times10^{-4}}\mathrm{e}^{-\tau^{0.027}} \tag{10}$$

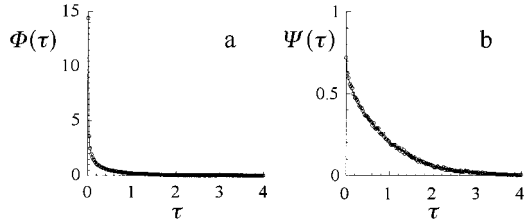

Figure 3. a) Simulation of the function $\Phi(\tau)$ obtained by the averaging of 1000 individual Brownian simulations, each one performed in dimensionless space using a set of $n = (4/3)\pi/\lambda^3$ particles disposed on a cubic network of lattice λ, with Brownian steps of length λ and duration λ^2, for $\lambda = 1/20$ and $\alpha = \pi\mathscr{H}(t)$, where $\mathscr{H}$ is the Heaviside unity step function; b) variations of $\Psi(\tau) = \Phi(\tau) \times \tau^{1/2}$ based on the simulated $\Phi(\tau)$.

The validity of the approximation in Equation (8) was then checked by examining the correlation between $\sigma_{\mathrm{recov}}(\tau)$ and $\sigma(\tau)$ in each case. In all cases a perfect correlation ($r \geq \sim 0.95$–0.98, data not shown) was observed provided only that the above requirement was met. These tests ensured that Equation (8) is valid over the whole range of experimental spikes. Furthermore, it is again verified during the analysis of a single spike (vide infra, Section B.II).

On the basis of the set of Equations (8)–(10), one may predict the shape of any spike that corresponds to a given $\sigma(\tau)$ opening function. Conversely, the same set allows extraction of the $\sigma(\tau)$ function that corresponds to a given spike expressed in dimensionless parameters (see Appendix B). However, several difficulties arise owing to the fact that the values of DRC/ε^3 and of $t_0 = R^2/D$ are unknown for this particular spike although they must be known in order to rescale the real current spike into the dimensionless space as required to solve Equation (8) (note that this was not a difficulty in the above tests since all the calculations were performed in the dimensionless space). Because of biological variations, these parameters are expected to vary significantly from their mean values, that is, even if their mean values have been estimated previously (C, R and ε) they cannot be used for the treatment of one particular spike. In the following section we explain how these difficulties can be overcome.

B. Application to experimental spikes

I. Determination of $t_0 = R^2/D$: An experimental spike is obtained as a digitized current vs. time function $i(t)$ (see Figure 1). The integration of this function up to infinite time affords the collected charge Q, which, as a result of the collection efficiency of unity, is a measurement of the initial amount of adrenaline molecules contained by the vesicle [Eq. (11)].

$$Q = \int_0^\infty i(t)dt = 2F \times N_0 = 2F \times \frac{4\pi}{3}R^3\left(\frac{C_0}{\varepsilon^3}\right) \tag{11}$$

On the other hand, numerically it is more convenient to work with normalized spikes, that is, with $I(t) = i(t)/i_{\max}$, since the maximum current $i_{\max}$ of the spike is easily available. Equation (8) is then rewritten in the real space as Equation (12), where $t_0 = R^2/D$, Ψ is given by Equation (10), and $\vartheta/4\pi$ is the derivative of the normalized opening function σ

$$I(t = \tau t_0) = \frac{i(t = \tau t_0)}{i_{\max}} = \frac{Q}{i_{\max}t_0} \times \int_0^\tau \frac{\Psi(\tau - \zeta)}{\sqrt{(\tau - \zeta)}}\frac{\theta(\zeta)}{4\pi}\mathrm{d}\zeta \tag{12}$$

[Eq. (9)]. Evaluation of the variation of the opening function $\sigma(t = t_0\tau)$ based on the numerical deconvolution of Equation (12) requires independent knowledge of t_0, yet this key parameter is not easily available from an experimental spike.

However, let us consider the structure of Equation (12) and the shape of a spike. From Equation (12), the spike shape arises from the convolution of two phenomena. The first, diffusion, is represented by $\Phi(\tau) = \Psi(\tau)/\sqrt{\tau}$ and is a rapidly decreasing component with an infinite branch at $\tau = 0$. The second, represented by $\vartheta(\tau)$, reflects the rate of unwrapping of the vesicle membrane by fusion to the cell membrane, namely, $\vartheta = (\mathrm{d}\sigma/\mathrm{d}\tau)4\pi$. σ, the fraction of the vesicle surface area

exposed to the extracellular fluid, is a steadily increasing function of time as observed by patch-clamp techniques (compare Figure 1), so that ϑ is expected to have a bell shape. This rationale explains why in a former work[5c] we used an exponentially modified gaussian model for treating $I(t)$, the gaussian component being a first-level approximation for the bell-shaped ϑ function and the exponential one being that for the rapidly decaying $\Phi = \Psi/\sqrt{\tau}$ function. The extremely satisfactory fitting of more than 200 differently shaped experimental spikes (sharp or broad ones) by this exponentially modified gaussian model therefore supports our present assumption on the bell shape of ϑ.

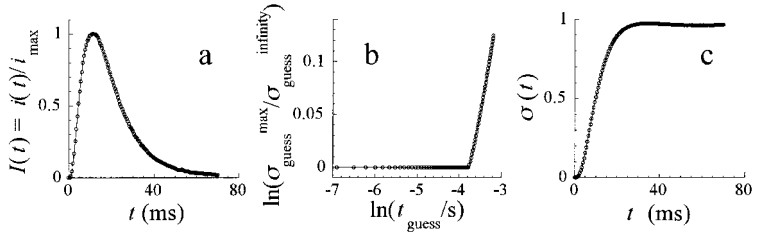

Figure 4. a) Normalized experimental current spike (viz., $I(t) = i(t)/i_{max}$) measured by amperometry during an individual exocytotic secretion event observed with a chromaffin cell stimulated by Ba^{2+}; b) variations of $\ln(\sigma^{max}_{guess}/\sigma^{\infty}_{guess})$ vs. $\ln(t_{guess})$ as obtained for the spike in a), and determination of t_0 by the intersection of the two linear regression lines ($t_0 = 23$ ms for the spike shown in a), see text; c) opening function $\sigma(t)$ extracted by deconvolution of Equation (12) applied to the data in a), based on t_0 determined in b).

Let us suppose now that one tries to solve Equation (12) using an estimated value (t_{guess}) of the unknown experimental parameter t_0. Two possibilities may occur. If $t_{guess} > t_0$, in the dimensionless space the current rises and decays faster than the actual value, since the dimensionless time used is compressed: $\tau_{guess} = t/t_{guess} < t/t_0 = \tau$. This will force $\sigma_{guess}(t)$, the solution of Equation (12) for t_{guess}, to increase too fast initially and then to decay to compensate artificially for the fact that the diffusional flux represented by $\Phi(\tau) = \Psi(\tau)/\sqrt{\tau}$ decays too smoothly with respect to $I(t_{guess}\tau)$. Thus when $t_{guess} > t_0$, the extracted function $\sigma_{guess}(t)$ is expected to present a maximum, a fact which would contradict the patch-clamp data (see, for example, Figure 1). Conversely, when $t_{guess} < t_0$, in the τ space the current rises and decays too slowly. $\sigma_{guess}(t)$ is then expected to lag behind the true $\sigma(t)$ function and therefore must rise steadily without presenting any maximum, because now the dimensionless time is dilated. Thus the correct t_0 value is the largest t_{guess} value for which the extracted function $\sigma_{guess}(t)$ presents no maximum, that is, for which $\sigma^{\infty}_{guess}/\sigma^{max}_{guess} = 1$, where σ^{∞}_{guess} is the limit of $\sigma(t)$ at large times and σ^{max}_{guess} the maximum value of $\sigma(t)$. This observation can be put into use for the automatic determination of t_0 from any spike with a good accuracy.

In practice, it is more advisable to perform this automatic determination using a log–log plot, since we noted empirically that when $t_{guess} > t_0$, $\ln(\sigma^{max}_{guess}/\sigma^{\infty}_{guess})$ is close to linear when plotted against $\ln(t_{guess})$. This property ensures fast determination of t_0 based on a simple linear regression (see Figure 4b), a process that is easily computerized. Therefore, the extraction of the opening function $\sigma(t)$ from a spike required a) the evaluation of Q and i_{max} from the experimental current/time $i(t)$ curve; b) a series of deconvolution procedures (see Appendix B) of Equation (12), which produce a series of $\sigma_{guess}(t)$ functions [Eq. (9)] for each guessed value t_{guess} of t_0; c) the determination of t_0 as explained above; d) the final and real deconvolution of Equation (12) using the determined value of t_0 to produce the real $\sigma(t)$ function. This sequence was fully computerized in C^{++} language, the starting estimated t_0 value being chosen as twice the half-width of the experimental spike. With a Pentium 333 MHz, the whole procedure took less than ca. 10 s per spike to produce the final $\sigma(t)$ and t_0.

II. Precision of the extraction procedure and improved extraction: In the previous section we have explained how the critical time parameter $t_0 = R^2/D$ can be evaluated for a given experimental spike. $\sigma(t)$ is then formally available from any current spike by means of Equations (9) and (12). However, a good precision on $\sigma(t)$ requires that the scaling parameters $\kappa = Q/(i_{max}t_0)$ and t_0 to be used in Equation (12) are likewise of good precision.

The main difficulty in evaluating κ with precision stems from the fact that although t_0 is evaluated through the above procedure with a precision better than a few percent (most generally by negative values observed empirically, vide infra), Q, the integrated charge of a current spike, is determined with an estimated precision of 10–20% percent, again by negative values because the spike current integration cannot be performed up to infinite times since either a) the spike is truncated because a second spike featuring a second distinct exocytotic event occurred before the current due to the first one had reached the base line, or b) because the current becomes too small and too close to the baseline after a few half-widths. The error in i_{max} (ca. 2%) is comparatively negligible. The resulting error in σ is thus expected to be of ca. 10–20% at most and to result mainly from the imprecision in Q. In practice, this precision may be estimated by the limit of $\sigma(t)$ at infinite time. This ought to correspond to 100% of the vesicle surface area (viz., $\lim \sigma(t) = 1$ for $t \to \infty$) if complete fusion occurs as is inferred from patch-clamp measurements. Indeed, nothing in the present model forces the vesicle to fully fuse with the membrane, so a poor precision of the overall extraction of $\sigma(t)$ may be reflected by the fact that the extracted function may well plateau before full opening, a scenario which seems a physical nonsense in the current view of exocytotic fusion events. In particular, owing to the structure of Equation (12), it is seen that an error in κ implies only a rescaling of $\sigma(t)$. All the approximately 600 different spikes treated through the procedure described in the previous section produced $\sigma(t)$ functions that reached their expected limit value at better than a few percent, a fact that shows that the error on κ was less than the above estimations because of partial error compensations.

When this precision is not sufficient or when the internal consistency of the procedure needs to be checked, a complete Brownian simulation of the problem can be performed. In the

© WILEY-VCH Verlag GmbH, D-69451 Weinheim, 1999
0947-6539/99/0507-2156 $ 17.50+.50/0 *Chem. Eur. J.* **1999**, *5*, No. 7

dimensionless space, a Brownian simulation requires $\sigma(\tau)$ as the input, so that both $\sigma(t)$ and t_0 are required. t_0 and the function $\sigma(\tau = t/t_0)$ that have been obtained at the end of the previous procedure can be used. Thus, the simulated current, $\varphi_{sim}(\tau)$, can be compared to the experimental normalized current $I(t) = i(t)/i_{max}$. From Equation (6) we can derive Equation (13). This comparison requires the simple adjust

$$I(t) = \kappa \times \varphi(t_0\tau) \tag{13}$$

ment of the two scaling parameters κ (viz., $\kappa = 1/\phi_{max}$) and t_0 so that the correlation between $I(t)$ and $I_{sim}(t)$ is the best possible (Figure 5, right column). Thus, a new set of κ and t_0 values, κ^{new} and t_0^{new}, can be generated in order that the maximum and half-width of the simulated $I_{sim}(t) = \kappa^{new} \times \varphi_{sim}(t_0^{new}\tau)$ coincide with those of the experimental $I(t)$. κ^{new} and t_0^{new} can then be used to generate a new σ function, σ^{new}, by numerical deconvolution of Equation (12); this σ^{new} can be used together with κ^{new} and t_0^{new} to perform a second Brownian simulation and the process repeated up to the point where κ^{new} and t_0^{new} remain invariant within the precision required. The

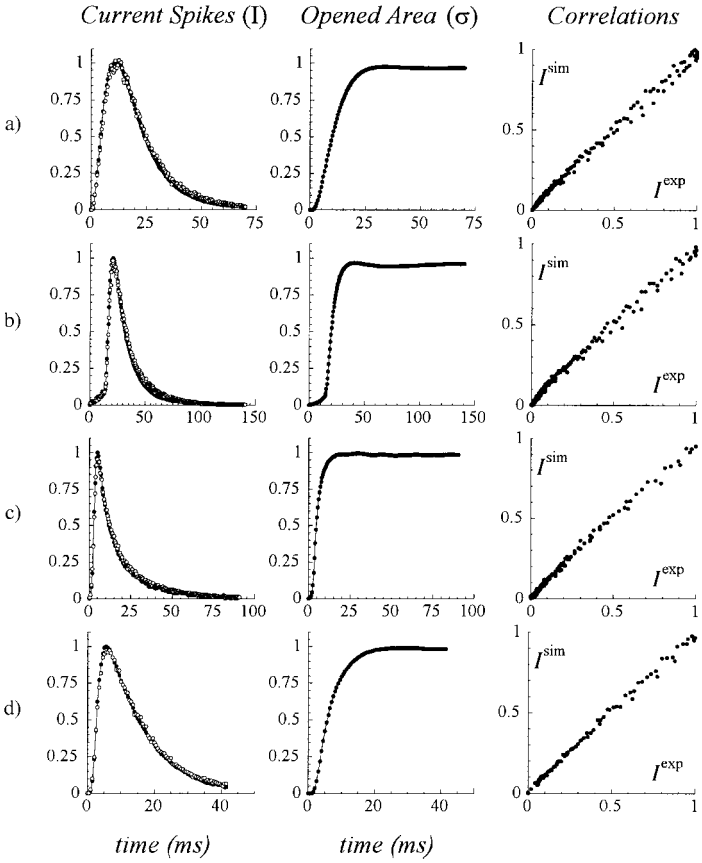

Figure 5. Left column (filled symbols): Normalized experimental current spikes ($I(t) = i(t)/i_{max}$) measured by amperometry during an individual exocytotic secretion event observed at a chromaffin cell stimulated by Ba^{2+}. Left column (open symbols): Normalized current spikes simulated by the Brownian procedure ($\lambda = 1/15$; 10 simulations averaged) on the basis of the $\sigma(t)$ functions shown in the middle column and $t_0 = 24.3$ (a), 30.1 (b), 33.1 (c), and 20.6 ms (d). Middle column: Variations of $\sigma(t)$, the normalized surface area of the vesicle exposed to the extracellular fluid during each of the exocytotic fusion events characterized by the current spikes shown in the left column. Right column: Correlation between simulated and experimental normalized current spikes.

final check of the method consists in examining the whole correlation between $I_{sim}(t)$ and $I(t)$ (see Figure 5, right column). In practice, five iterations at most were required, and resulted in t_0 values that increased by less than a few percent compared with their estimation by the convolution integral procedure, while Q could increase by as much as 10%, depending on the quality of the experimental current integration. Again, the iterative process was fully computerized (C^{++} language). It took less than 5 to 10 min per spike and per iteration on a Pentium 333 MHz. Each simulation was in fact the average of 10 Brownian-independent simulations performed with $\lambda = 1/15$ (see Appendix A) in order to reduce the Brownian noise at long times. Much faster procedures involving no averaging per Brownian simulation (30 s to 1 min per iterative step) can be used, in particular during the first iteration steps, since the long time branch is not used in the rescaling procedure as this requires only I_{max} and $t_{1/2}$. Also, Brownian procedures could be interrupted after $t_{1/2}$ (15 to 30 s per iterative step). Nevertheless, we preferred to use the longer iterative procedure at each iterative step since the time consumption was not a problem for us.

Figure 5 shows the result of this iterative procedure as applied to four different spikes selected for their very different shapes and the different problems they pose so as to be illustrative of the variety observed experimentally for the approximately 600 different spikes that have been treated. As illustrated by this representative set, the agreement between experimental and simulated spikes is excellent. However, it should be emphasized that although the iterative procedure improved the correlation between $I_{sim}(t)$ and $I(t)$, we observed that for most of the well-behaved spikes, that is, for those in which the charge integration can be performed with a reasonable accuracy and whose rising part is described with sufficient time resolution (e.g., as in Figure 5a), the iterative procedure was not necessary because the first procedure was sufficiently accurate. Conversely, for the poorly behaving spikes the iterative procedure improved the fit between experimental and simulated currents. Figures 5b–d illustrate the effectiveness of the iterative procedure by presenting its final result on three representative poorly behaving spikes. Thus even spikes in which the rising branch is merged with a foot component (Figure 5b),[16a] or with a poorly time-resolved rising branch (Figure 5c) and even truncated spikes (Figure 5d) in which Q cannot be determined to a good precision through simple current integration can be processed adequately.

C. Final comments

The parameters κ and t_0 are determined as part of the extraction procedure leading to the opening function $\sigma(t)$. Although we focused in this work on the extraction of $\sigma(t)$ from experimental spikes, it should be noted that κ and t_0 are rich in physicochemical information on the vesicle. Indeed, $\langle t_0 \rangle = \langle R^2/D \rangle$ gives the mean diffusion coefficient of adrenaline in the swollen matrix, since $\langle R_0 \rangle = 150$ nm and $\langle \varepsilon \rangle = 1.35$ are known. Similarly, $\langle \kappa i_{max} t_0 \rangle / 2F = \langle Q \rangle / 2F = \langle N_0 \rangle$ is the initial mean content of adrenaline inside the vesicle, which gives access to its internal initial mean concentration $\langle C_0 \rangle$. How-

ever, such statistical data have to be determined from the treatment of a large series of spikes. Such analyses will be reported in a forthcoming paper[17] since this one is devoted mostly to the presentation of the theory and the principle of the extraction procedures. They led to $\langle D\rangle \approx 4.1 \times 10^{-8}\,\mathrm{cm^2\,s^{-1}}$, $\langle N_0\rangle \approx 9$ attomoles, and $\langle C_0\rangle \approx 0.60$ M, that is, to values that are consistent with previous determinations ($\langle N_0\rangle$ and $\langle C_0\rangle$)[4h, 5c] or for the expected diffusion coefficient within a swollen polyelectrolyte matrix.[12b]

We wish to focus our discussion here on the very particular time-shape of the $\sigma(t)$ function since, to the best of our knowledge, this is the first time that this function could be determined with such precision and time resolution. The shapes illustrated in the middle column of Figure 5 are perfectly representative of all those found for the series of ca. 600 spikes treated. As expected and inferred from patch-clamp experiments, $\sigma(t)$ has a sigmoidal shape. Yet one notices immediately the profound disymmetry between the temporal behaviors at short and long intervals. At short intervals, $\sigma(t)$ consistently expands with a kind of explosive or autoaccelerated kinetic character, a feature that is maintained nearly up to the half-unwrapping of the vesicle. The remainder of the vesicle unwrapping proceeds with a much smoother pace and has the shape expected for the resorption of a curvature in a membrane.

Although a proper discussion of this peculiar behavior requires a statistical treatment based on numerous spikes, treatment that will be reported later together with the aforementioned analyses, we wish to make some proposals here that may explain this behavior and may have important consequences for the rationalization of the passage from the pore release to the spike.

Let us consider the simple model in Figure 2. As explained and justified above, in the present work based on this model, the spherical symmetry of the vesicle could be conserved because we supposed the swelling to be sufficiently fast for the kinetics inside the vesicle to be controlled by diffusion only. In this model, swelling is thus kinetically and geometrically transparent and allows only the diffusion coefficient of the adrenaline cation to pass from nearly zero in the unswollen matrix zones to a significant value ($\langle D\rangle \approx 4 \times 10^{-8}\,\mathrm{cm^2\,s^{-1}}$) in the swollen ones. However, let us consider now the more realistic views sketched in Figure 6. When $\alpha < \pi/2$ (Figure 6a) the convexity of the system means that the pressure increase due to the matrix swelling creates a force that applies on the membrane edges around α. This force contributes positively and adds to all the others that provoke the resorption of the curvature of the vesicle membrane, so that the rate of unwrapping is expected to be faster than when such forces do not apply. Moreover, this faster unwrapping opens faster new domains of the vesicle wall to hydration and ion exchange with the extracellular fluid, domains which then swell faster and add to the force, and so on, so that the unwrapping rate accelerates. Conversely, when $\alpha > \pi/2$ (Figure 6b), the system becomes concave and the resulting force due to the matrix swelling is no longer directed towards the membrane edge but towards the top of the figure where expansion occurs freely by simple displacement of the extracellular fluid. Thus the kinetics of the membrane unwrapping is expected to slow down and to behave as expected for a normal elastic resorption of a membrane curvature. Thus, these simple intuitive considerations on the different effects of the pressure forces created by the swelling as a function of the convexity ($\alpha < \pi/2$) or the concavity ($\alpha > \pi/2$) of the system geometry explains qualitatively the peculiar behavior of $\sigma(t)$.

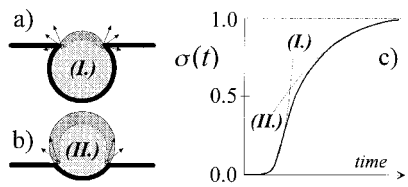

Figure 6. Schematic representation of the effect of the forces (shown as arrows) exerted by the matrix swelling according to the convexity of the system, i.e., as a function of α. a): Case I (first half of membrane unwrapping: $0 \le \alpha \le \pi/2$). b): Case II (second half of membrane unwrapping: $\pi/2 \le \alpha \le \pi$). The swollen matrix is deeply shaded, while the unswollen domain is lighter. In c) the variations of $\sigma(t)$ are sketched with the two limiting behaviors indicated in dashed lines: accelerated fusion (case I, see a) and normal fusion (case II, see b); see text.

The same consideration on the crucial role of the swelling pressure may be applied to the transition between the foot and spike modes of release. Indeed, during the pore release, the architecture of the pore/membrane assembly is maintained by the cohesion energy E_{channel} of the ionic channel and of its attachment to the cell and vesicle membrane.[4f] However, each catecholamine cation released through the pore is necessarily replaced inside the vesicle by hydrated ions from the extracellular fluid to satisfy electroneutrality. As explained above, this exchange disrupts the polyelectrolyte cohesion and is thus expected to provoke the swelling of the zone altered. However, this altered zone should not swell totally (that is, as during the spike release) because of the space constriction, so that a significant compression energy has to develop in this zone, being proportional to the number of sites altered in the polyelectrolyte matrix. If the alteration of the matrix structure by hydration and cation exchange corresponds to an energy ΔE_{alt} per site altered, and ΔN sites are altered, the accumulated energy is $\Delta N \times \Delta E_{\mathrm{alt}}$. Considering that the pore has opened during Δt, $\Delta N \approx i_{\mathrm{foot}}\Delta t/(2F)$, where i_{foot} is the constant foot plateau current. Since i_{foot} is ≈ 5 pA,[4h, 5c] approximately 10^4 sites are altered per millisecond. Since $\langle C_0\rangle = 0.6$ M, this corresponds to a rate of volume alteration of ca. $3 \times 10^4\,\mathrm{nm^3\,ms^{-1}}$. The radius of the unswollen vesicle $\langle R_0\rangle$ being ~ 150 nm, this corresponds to a significant alteration of the matrix. Every millisecond it affects a domain of ca. 2‰ of the initial vesicle volume, a domain whose radius is ca. 20 nm (specifically, 18 nm if the altered zone is spherical or 22 nm if it is a hemispherical capsule centered on the entrance of the pore).

Therefore, a pressure energy of ca. $10^4\,\Delta E_{\mathrm{alt}}$ builds up every millisecond inside the matrix. This corresponds to an energy $10^4\,\Delta E_{\mathrm{alt}}\,(R_{\mathrm{pore}}/R_{\mathrm{o}})^2 \sim \Delta E_{\mathrm{alt}}$ over the surface area of the pore. It is thus expected that when the pore duration reaches $\Delta t_{\mathrm{max}}\,(\mathrm{ms}) = (\Delta E_{\mathrm{channel}}/\Delta E_{\mathrm{alt}})$, the system reaches a threshold point where the ionic channel architecture cannot hold the increasing pressure any longer, so that it may have to close or blow apart in order to release the internal pressure. Indeed, since most of the pressure has to be localized near the docking

 © WILEY-VCH Verlag GmbH, D-69451 Weinheim, 1999 0947-6539/99/0507-2158 $ 17.50+.50/0 *Chem. Eur. J.* **1999**, *5*, No. 7

point because it can only with difficulty be evacuated by diffusion into the unswollen matrix, we presume that the release of the accumulated energy will occur mostly in this area. The resulting local nanoscopic explosion is then expected to provide sufficient energy to bring up local disorder in the face-to-face phospholipidic bilayers of each membrane. By such a mechanism the electrostatic repulsion between the negative heads of each phospholipidic bilayer should be easily avoided. Thus, the fusion of the two membranes may start by simple relaxation of the system after the explosion.

For chromaffin cells, we estimate Δt_{max} to be of the order of 2 ms from the amperometric results,[5d] so that we obtain $\Delta E_{channel}/\Delta E_{alt} \sim 1$.

To conclude this discussion, it is interesting to note that if one assumes that this figure is invariant for all kind of secretory catecholamine vesicles which contain matrixes similar to those of adrenal cells, a vesicle that contains less than ca. $\langle N_{max} \rangle \sim 2 \times 10^4$ molecules of neurotransmitter should never be able to reach the point where fusion may start. Indeed, the pore/membrane architecture will have enough strength to hold the internal pressure even when the vesicle is fully emptied. Compared with $\langle R_0 \rangle \sim 150$ nm and $\langle N_0 \rangle = 5 \times 10^6$ molecules for chromaffin vesicles, this threshold figure corresponds to a maximum radius of ca. $\langle R_{max} \rangle \sim 25$ nm. In other words, on the basis of these considerations, a vesicle with a radius smaller than 25 nm should be able to empty itself completely through its pore without accumulating sufficient compression energy to exceed that of the pore/membrane architecture. Therefore, it should never be able to fuse spontaneously. Conversely, a secretory vesicle with a radius exceeding significantly 25 nm should always end by fusing unless another mechanism closes the pore before the threshold energetic point is reached. Although one should keep in mind the still rudimentary aspects of this discussion and its possible overgeneralization since it assumes an energetic likeness between the inner components of different kinds of vesicles and between their pore/membrane architectures, it is interesting that the two above threshold limits, $\langle N_{max} \rangle \sim 2 \times 10^4$ molecules and $\langle R_{max} \rangle \sim 25$ nm, are surprisingly close to the values reported for synaptic cholinergic vesicles in neurons, namely $\langle N \rangle \sim 10^4$ molecules and $\langle R \rangle \sim 20 \sim 30$ nm.[18] In other words, if this rudimentary prediction holds, synaptic vesicles in neurons would be the largest vesicle possible that will allow exocytosis without fusion; that is to say, in this respect they would be the optimized exocytotic system in synapses.

Conclusion

In this work we have presented a method which allows the extraction of the variations of the opening function $\sigma(t)$ from an experimental amperometric current spike featuring an individual exocytotic secretion event. This method is based on the recognition that the overall spike shape results from the convolution of this opening function, which regulates the fraction of the vesicle surface area that is exposed to the extracellular fluid by a diffusion function that features the diffusion and exchange of the catecholamine cation inside the matrix core of the vesicle. This convolution can be treated mathematically to yield a convolution integral formulation based on an approximation on the relative time scales of the opening function and diffusion. It may also be treated numerically without the need for this simplifying approximation by means of Brownian motion simulations. Despite its better value because it involves a less approximated level, the Brownian motion simulation approach requires the opening function $\sigma(t)$ function as its input. Conversely, the convolution integral approach affords the $\sigma(t)$ function as its output. Iterative combination of the two approaches thus permits the extraction of the opening function with an excellent precision and a resolution that has never been achieved before. As a correlate of this analysis, several other parameters which control the exocytotic physicochemical behavior are also obtained, but as their analysis requires the statistical treatment of a sufficient number of spikes these results will be reported later.

The peculiar shape of the opening functions $\sigma(t)$ hints at the fact that the exocytotic events are intimately regulated by the swelling of the matrix polyelectrolyte core of the vesicle, although this important component is transparent in the analysis proposed here. Indeed, depending on the extent of the fusion, that is, whether the vesicle is less or more than half-unwrapped, the convexity of the system changes. Thus, the forces created by the gel matrix swelling accelerate the unwrapping of the vesicle during the first phase when the system is convex, while it plays a lesser role during the second phase because the system is concave. This dichotomy is reflected by the opening function $\sigma(t)$, which increases in an explosive fashion during the first phase but slows down considerably during the second phase.

This observation points to the important role of the matrix swelling in the whole exocytotic behavior. In particular, this effect may be elaborated in order to offer a possible new energetic interpretation of the transition between pore release and fusion release for those cells which contain polyelectrolyte matrixes similar to those of adrenal cells. On this basis, and assuming rather similar energetic behavior for all kind of catecholamine secretory vesicle matrixes, secretory vesicles can be separated into two classes according to their radius and catecholamine content. Vesicles with a radius of less than $\approx$25 nm and containing less than ca. 20000 molecules of catecholamines should never be able to accumulate a sufficient compression energy to reach the explosion threshold energetic point, so that they should always release through channel docking. The other vesicles should always end up fusing with the cell membrane, unless another mechanism closes the pore before about ten thousand molecules of catecholamines have been released.

Experimental Section

All the programs developed in this work were written in C^{++} and ran on a Pentium 333 MHz PC. The codes are available from the authors on demand.

The current spikes presented in this work (Figure 4a and Figure 5, left column a–d) were recorded by Eric Travis in Prof. R. Mark Wightman's group (University of North Carolina, Chapel Hill, USA). They served here to establish the validity and the performances of the present analysis, since

they are representative of a series of ≈600 spikes which were recorded in Wightman's group and treated in our group with the present method in the context of a collaborative work that will be reported later.[17] The five spikes used here are shown with Wightman and Travis's kind permission. The following experimental details describe how the experiments were conducted in Wightman's group, and they are reported here with his permission only for the reader's information.

The spikes were recorded as previously described[6b] from bovine adrenal medullary (chromaffin) cells maintained in primary cultures. Experiments were performed at $23.0 \pm 0.1\,^{\circ}C$ between days 4 and 5 of culture. In the experiments, the culture medium (Dulbecco's modified Eagle's medium/Ham's F12 medium, from Gibco Laboratories, Grand Island, NY, USA) was replaced by a solution containing NaCl (154 mM), KCl (4.2 mM), $MgCl_2$ (0.7 mM), glucose (11.2 mM), and 4-(2-hydroxyethyl)-1-piperazineethanesulfonic acid (HEPES, 10 mM) brought to pH 7.4 with NaOH addition. Exocytosis was elicited by 5-second pressure ejection of 5 mM Ba^{2+}.[3c,d, 5a] Flame-etched carbon-fiber microelectrodes (ca. 5 μm tip radius) were constructed as described elsewhere.[19] To ensure the bielectronic oxidation of adrenaline, the electrode potential was set at +0.650 V vs. SSCE (saturated sodium calomel electrode). The electrochemical spikes were measured with patch-clamp electronic equipment (Axopatch 200B, Axon Instruments). The amperometric current was digitized to videotape and later filtered through a fourth-order, low-pass (400 Hz) filter (CyberAmp 320, Axon Instruments), digitized at 0.5 ms/point and stored on a PC hard drive. The digitization rate and filter frequency were selected so that distortion of the temporal characteristics did not occur.

Acknowledgments

This work has been supported in parts by CNRS (UMR CNRS 8640 PASTEUR), by the Ecole Normale Supérieure, and by the French Ministry of Research and Education (MENRT). Prof. Wightman and Eric Travis are gratefully acknowledged for kindly supplying to us the five current spikes shown in Figure 4a and in the left column of Figure 5.

Appendices

Appendix A. Brownian motion simulations: All the Brownian simulations were performed in the dimensionless space [see Eqs. (2)–(5)]. Thus the matrix is represented by a sphere of radius unity and the dimensionless diffusion coefficient is unity. The length step is λ and therefore the time step is λ^2. For ease and to ensure a homogeneous filling of the unit sphere, ca. $(4/3\lambda^3)\pi$ particles were positioned on a cubic network of lattice $1/\lambda$. It was checked that this procedure did not change the results by comparison to a random positioning of the ca. $(4/3\lambda^3)\pi$ particles in the unit sphere. A random vector $\vec{\mathbf{v}}$ is sorted at each time step for each particle and the particle is moved by $\vec{\mathbf{v}}/(\lambda\,|\,\vec{\mathbf{v}}\,|)$. This is repeated up to the time τ when the particle exits the sphere through the permeable area which is imposed by $\alpha(\tau)$. Then the particle is counted and added to the flux $\varphi(\tau)$ at time τ. If the particle hits the sphere wall at a time τ where the wall is still impermeable as imposed by $\alpha(\tau)$, it is bounced back using a perfect reflection condition so that its overall step length remains λ.

The step length λ influences the precision of $\varphi(\tau)$, since there are $1/\lambda^2$ time points per unit of dimensionless time τ. Because the initial filling of the sphere is also regulated by λ—there are $(4/3\lambda^3)\pi$ particles—this parameter also controls the random noise in $\varphi(\tau)$ counts. To increase the signal-to-noise ratio, either the lattice of the cubic network could be decreased by a factor Λ, by considering ca. $[4/3(\lambda\Lambda)^3]\pi$ particles, or by performing Λ^3 identical simulations and averaging the Λ^3 independent $\varphi(\tau)$ after a while. For convenience we chose the second solution. For the simulation of $\Phi(\tau)$ we used 1000 independent simulations ($\lambda = 1/20$) since we needed an extremely accurate solution at short and long times (see text), while for the simulations of the current spikes (Figure 5) averaging 10 independent simulations (with $\lambda = 1/15$) gave adequate precision.

For the tests of validity of the convolution integral formulation, sigmoidal $\sigma(\tau)$ functions were generated: $\sigma(\tau) = 1/\{1 + \exp - [k(\tau - \tau_{1/2})]\}$, where k was varied ($0.2 \le k \le 2$) to cover a range of spike shapes that encompassed the experimentally observed ones. $\tau_{1/2} = 5/k$ was adjusted in each case so that $\sigma(\tau) < 10^{-2}$ for $\tau = 0$. These functions were used to perform Brownian simulations ($\lambda = 1/15$, 10 simulations average) to yield a series of simulated current spikes $\varphi(\tau)$. Each of these simulated current spikes was deconvoluted (vide infra, Appendix B) with Equation (8) to give a corresponding series of $\vartheta_{recov}(\tau)$ functions, from which the series of $\sigma_{recov}(\tau)$ functions were obtained through application of Equation (9). The correctness of Equation (8) was then ascertained by examining the correlation between $\sigma_{recov}(\tau)$ and the input function $\sigma(\tau)$ for each k value, as represented for $I(t)^{sim}$ vs. $I(t)^{exp}$ in the right column of Figure 5 (correlation coefficients were between 0.95 and 0.98). Furthermore, it is noted that the convergence of the iterative procedure described in the text (Section B.II of Results and Discussion) provides another series of positive tests of the validity of Equation (8), this time for real current spikes.

Appendix B. Numerical deconvolution of Equations (8) or (12): The procedure used is adapted from a previous classical work from this group in the context of electrochemical problems.[20] It consists in rendering the convolution integral in Equation (8) or (12) discrete with a dimensionless time step $\Delta\tau$ that: a) is imposed by the experimental digitizing time interval (0.5 ms) of the experimental spikes and by t_0, namely, $\Delta\tau = \Delta t//t_0 = 0.5/(t_0/\text{ms})$, or b) was selected as a function of k, $\Delta\tau = 1/20k$, during the test of validity of Equation (8), so that the input $\sigma(\tau)$ was properly defined. Thus, at any time $\tau = m\Delta\tau$, Equation (8) or (12) can be rewritten as Equation (B1), where $\tilde{\varphi}(\tau) = 4\pi\varphi(\tau)$ for the dimensionless Equation (8), or $\tilde{\varphi}(\tau) = 4\pi(i_{max}t_0/Q) \times I(t = \tau t_0)$ for Equation (12). Note that in Equation (8), $\Phi(\tau)$ must be replaced by $\Psi(\tau)/\sqrt{\tau}$ for its resolution by the following procedure.

$$\tilde{\varphi}(\tau) = \int_0^{\tau} \Psi(\tau-\zeta)\vartheta(\zeta)\frac{d\zeta}{\sqrt{\tau-\zeta}} \approx \sum_{n=0}^{n=(m-1)} \left[\int_{n\Delta\tau}^{(n+1)\Delta\tau} \Psi(\tau-\zeta)\vartheta(\zeta)\frac{d\zeta}{\sqrt{\tau-\zeta}}\right] = \sum_{n=0}^{n=(m-1)} \chi_n \qquad (B1)$$

Over the time interval $[n\Delta\tau,(n+1)\Delta\tau]$, Ψ and ϑ are linearized, and the resulting analytical integral χ_n is integrated analytically. Thus, noting $\Psi_n = \Psi(n\Delta t)$ and $\vartheta_n = \vartheta(n\Delta t)$, one obtains Equations (B2) and (B3) for $\zeta \in [n\Delta\tau,(n+1)\Delta\tau]$. As a result, Equation (B4) holds [A_n, B_n, and C_n are

$$\Psi(\tau-\zeta) = \Psi_{m-n} + (\Psi_{m-n-1} - \Psi_{m-n})(\zeta - n\Delta t)/\Delta t \qquad (B2)$$

$$\vartheta(\zeta) = \vartheta_n + (\vartheta_{n+1} - \vartheta_n)(\zeta - n\Delta t)/\Delta t \qquad (B3)$$

$$\chi_n = \Delta t^{1/2} \times \{A_{m-n}\vartheta_n\Psi_{m-n} + B_{m-n}\,[\vartheta_n(\Psi_{m-n-1} - \Psi_{m-n}) + \Psi_{m-n}(\vartheta_{n+1} - \vartheta_n)] + C_{m-n}(\vartheta_{n+1} - \vartheta_n)(\Psi_{m-n-1} - \Psi_{m-n})\} \qquad (B4)$$

defined in Eqs. (B5)–(B7)], so that at each time step $\tau = m\Delta\tau$, $\vartheta_m = \vartheta(m\Delta t)$, for $m > 1$, is obtained explicitly as the solution of the linear

$$A_n = \frac{1}{\Delta\tau^{1/2}}\int_0^{\Delta\tau}\frac{d\zeta}{\sqrt{n\Delta\tau-\zeta}} = 2[n^{1/2} - (n-1)^{1/2}] \qquad (B5)$$

$$B_n = \frac{1}{\Delta\tau^{3/2}}\int_0^{\Delta\tau}\frac{\zeta d\zeta}{\sqrt{n\Delta\tau-\zeta}} = \frac{4}{3}[n^{3/2} - (n-1)^{3/2}] - 2(n-1)^{1/2} \qquad (B6)$$

$$C_n = \frac{1}{\Delta\tau^{5/2}}\int_0^{\Delta\tau}\frac{\zeta^2 d\zeta}{\sqrt{n\Delta\tau-\zeta}} = \frac{2}{3}\left\{\frac{8}{5}[n^{5/2} - (n-1)^{5/2}] - (4n-1)(n-1)^{1/2}\right\} \qquad (B7)$$

Equation (B8), where D_m is as defined in Equation (B9), with $\tilde{\varphi}_m = \tilde{\varphi}(m\Delta\tau)$. For $m = 1$, we obtain Equation (B10).

$$\vartheta_m = [(15/\Psi_1)D_m - \vartheta_{m-1}(6 + 4\Psi_0/\Psi_1)]/(4 + 16\Psi_0/\Psi_1) \qquad (B8)$$

$$D_m = \frac{1}{\sqrt{\Delta\tau}}\left[\tilde{\varphi}_m - \sum_{n=0}^{n=(m-2)}\chi_n\right] \qquad (B9)$$

$$\vartheta_1 = [(15/\Psi_1)/(4 + 16\Psi_0/\Psi_1)]\tilde{\varphi}_1/\sqrt{\Delta\tau} \qquad (B10)$$

Iterative application of Equation (B8), starting with $\vartheta_0 = 0$ and ϑ_1 given by Equation (B10), affords the successive values ϑ_m of $\vartheta(\tau)$ at each time mesh point $\tau = m\Delta\tau$. The values of $\sigma(\tau)$ or of $\alpha(\tau)$ at each point are then readily

© WILEY-VCH Verlag GmbH, D-69451 Weinheim, 1999
0947-6539/99/0507-2160 $ 17.50+.50/0 *Chem. Eur. J.* **1999**, *5*, No. 7

obtained through Equation (9) by trapezoidal numerical integration of $\vartheta(\tau)$. It is noted that the values $\Psi_0 = \Psi(\tau = 0)$ and $\Psi_1 = \Psi(\tau = \Delta\tau)$ play a crucial role at each step because of their involvement in Equations (B8) and (B10). This is why great care must be taken in evaluating the function $\Psi(\tau)$ and its empirical analytical approximation in Equation (10). Similarly, if the solution of Equations (8) or (12) had relied on $\Phi(\tau)$ [as strictly written in Eq. (8)] instead of $\Psi(\tau)/\sqrt{\tau}$ as given above [Eq. (B1)], an equation similar to Equation (B8) would have been obtained, but instead with the values $\Phi_0 = \Phi(\tau \to 0)$ and $\Phi_1 = \Phi(\Delta\tau)$ of $\Phi(\tau)$, which cannot be determined because $\Phi(\tau)$ has an asymptotic branch at $\tau \to 0$. With the present formulation, the problem does not arise because the analytical integrations in Equations (B5) – (B7) eliminate the infinite branch problem.

Appendix C. The Φ function: The extraction of $\sigma(\tau)$ from an experimental spike thanks to Equations (6), (8), and (9), requires the independent knowledge of the function $\Phi(\tau)$. This function should be rather classical since it corresponds to the diffusional emptying of a sphere under the condition of zero concentration on its wall. However, we have not been able to locate any trace of such a function in the literature. Therefore we had to determine this function; we chose to achieve a numerical solution through Brownian motion simulation.

The main difficulty is the evaluation of $\Phi(\tau)$ at short times τ. Indeed, by analogy with the Cottrellian flux to a plane,[15] $\Phi(\tau)$ must present an infinite branch at short times; specifically, $\Phi(\tau) \propto \tau^{-1/2}$ when $\tau \to 0$. This is precisely the time domain where any numerical simulation (Brownian motion or finite differences) is less precise. Furthermore, it is clear from the structure of Equation (8) that Φ must be very precise in the short time ranges, since then Φ has its largest weight in the convolution integral. To achieve the necessary extremely accurate solution of Φ at short times, it is preferable to evaluate $\Psi(\tau) = \Phi(\tau)\tau^{1/2}$ rather than $\Phi(\tau)$, since, on the basis of the Cottrellian analogy, $\Psi(\tau) \to \Psi_0$ when $\tau \to 0$, where Ψ_0 is a constant. This is not detrimental because either Equation (8) can be rewritten accordingly or $\Phi(\tau)$ determined analytically from $\Psi(\tau)$.

A strict Cottrellian analogy (viz., planar diffusion limit at short times) would readily give $\Psi_0 = 3\pi^{-1/2}$.[15] However, even at short times when the dimensionless thickness of the diffusion layer is much less than unity (i.e., than the vesicle dimensionless radius) the diffusion problem cannot be assimilated to the planar case because of the concavity of the sphere. Indeed, in such a case a particle located on the very wall of the sphere does not have a 50% chance of exiting the sphere after one Brownian step of infinitely short length, in contrast to what occurs for a plane. To establish this, let us consider a particle located in the sphere at a distance δ (in the dimensionless space) from the wall. By geometrical construction (from the ratio of solid angles), the probability $\Omega(\delta)$ that this particle exits the sphere at the next Brownian step of length λ and duration $\theta = \lambda^2$ (note that D is unity in the dimensionless space, so that $\theta = \lambda^2/D = \lambda^2$) is given by Equation (C1) if $0 \le \delta \le \lambda$, or is zero when $\lambda \le \delta$. At $t = 0$, the concentration

$$\Omega(\delta) = \tfrac{1}{2}\{1 + (\lambda^2 + \delta^2 - 2\delta)/[2\lambda(1-\delta)]\} \tag{C1}$$

is still homogeneous within the sphere, and equal to $3/4\pi$ in dimensionless units, since $\eta(\tau = 0) = 1$ by definition [Eq. (4)]. The fraction $\Delta\eta$ of particles exiting from the sphere during the Brownian step of duration λ^2 (in the dimensionless time scale) is then given by Equation (C2), the flux of particles that exit the sphere during this step being $\Delta\Phi = \Delta\eta/\lambda^2$, thus $\Psi_0 = \lim_{\lambda \to 0}(\Delta\eta/\lambda) = 3/4$.

$$\Delta\eta = \frac{3}{4\pi}\int_0^{\lambda} \Omega(\delta) \times 4\pi(1-\delta)^2 \mathrm{d}\delta = \frac{3\lambda}{4} - \frac{\lambda^3}{32} \tag{C2}$$

The second difficulty in Brownian motion evaluation of $\Phi(\tau)$ or $\Psi(\tau)$ arises at infinite times. Indeed, in simulations of such conditions the flux of particles exiting from the sphere becomes vanishingly small so that the $\Phi(\tau)$ or $\Psi(\tau)$ Brownian values becomes chaotic when $\tau \gg 1$, because the Brownian noise then becomes larger than the signal. This important difficulty can be eliminated: Owing to the conservation of matter, the number of particles that exit from the sphere over an infinite time is equal to the initial content of the sphere. Since $\eta(\tau = 0) = 1$, $\Phi(\tau)$ and $\Psi(\tau)$ must then obey the normalization requirement of Equation (C3).

$$\eta(\tau = 0) = \int_0^{\infty} \Phi(u)\mathrm{d}u = \int_0^{\infty} \frac{\Psi(u)}{\sqrt{u}}\mathrm{d}u = 1 \tag{C3}$$

Up to $\tau = 5$, 1000 Brownian simulations were performed and averaged to decrease the Brownian noise at longer times. Each simulation was performed with $\lambda = 0.05$ (i.e., with a step time 2.5×10^{-3}) and starting from a set of ca. $(4/3)\pi/\lambda^3$ particles located homogeneously within the sphere on a cubic network of lattice λ. The results are shown in Figure 3 in terms of $\Phi(\tau)$ and $\Psi(\tau)$. Based on these results, the analytical empirical expression of $\Psi(\tau)$ given in Equation (10) and which obeys the two above conditions [Eq. (C3) and $\Psi_0 = 3/4$] was developed in order to facilitate the numerical resolution of Equation (8).

[1] a) B. Uvnäs, C. H. Åborg, *News Physiol. Sci.* **1989**, *4*, 68; (b) B. Uvnäs, C. H. Åborg, *Acta Physiol. Scand.* **1983**, *119*, 225.

[2] a) J. R. Monck, A. F. Oberhauser, G. Alvarez de Toledo, J. M. Fernandez, *Biophys. J.* **1991**, *59*, 39; b) C. Nanavati, J. M. Fernandez, *Science* **1993**, *259*, 963.

[3] a) L. von Ruden, E. Neher, *Science* **1993**, 262, 1061; b) R. S. Zucker, *Neuron* **1996**, *17*, 1049. For Ba^{2+} stimulation see: c) L. von Ruden, A. G. Garcia, M. G. Lopez, *FEBS Lett.* **1993**, 336, 48; d) D. A. Przywara, P. S. Chowdhury, S. V. Bhave, T. D. Wakade, A. R. Wakade, *Proc. Natl. Acad. Sci. USA* **1993**, *90*, 557.

[4] a) L. J. Breckenridge, W. Almers, *Nature* **1987**, *328*, 814; b) A. E. Spruce, L. J. Breckenridge, A. K. Lee, W. Almers, *Neuron* **1990**, *4*, 643; c) R. H. Chow, L. von Ruden, E. Neher, *Nature* **1992**, *356*, 60; d) J. R. Monck, J. M. Fernandez, *J. Cell Biol.* **1992**, *119*, 1395; e) J. R. Monck, J. M. Fernandez, *Neuron* **1994**, *12*, 707; f) K. Lollike, N. Borregaard, M. Lindau, *J. Cell Biol.* **1995**, *129*, 99; g) J. R. Monck, J. M. Fernandez, *Current Opin. Cell Biol.* **1996**, *8*, 524; h) J. A. Steyers, H. Horstmann, W. Almers, *Nature* **1997**, *388*, 474; i) A. Albillos, G. Dernick, H. Horstmann, W. Almers, G. Alvarez de Toledo, M. Lindau, *Nature* **1997**, *389*, 509.

[5] a) J. A. Jankowski, J. M. Finnegan, R. M. Wightman, *J. Neurochem.* **1994**, *63*, 1739; b) R. M. Wightman, T. J. Schroeder, J. M. Finnegan, R. L. Ciolkowski, K. Pihel, *Biophys. J.* **1995**, *68*, 383; c) T. J. Schroeder, R. Borges, J. M. Finnegan, K. Pihel, C. Amatore, R. M. Wightman, *Biophys. J.* **1996**, *70*, 1061; d) considering that all foot components observed in these references result from a unique mechanism, and taking into account that an average of 25% of exocytotic events lead to a mean foot duration of 8 ms, the mean foot duration for all events is $\Delta t_{mean} = 0.25 \times 8\ (\mathrm{ms}) + 0.75 \times \Delta t_{0.5}\ (\mathrm{ms})$, where $\Delta t_{0.5}$ is the mean foot duration for the fraction of events in which the duration of the foot is less than our time resolution of 0.5 ms. Since $\Delta t_{0.5}$ is necessarily between 0 ms and 0.5 ms, Δt_{mean} is between 2 ms (i.e., if $\Delta t_{0.5} \ll 0.5$ ms) and 2.4 ms (i.e., if $\Delta t_{0.5} = 0.5$ ms), so $\Delta t_{mean} = (2.2 \pm 0.2)$ ms.

[6] a) For a review of the principle of artificial synapses see: C. Amatore, *C.R. Acad. Sci. Ser. IIb* **1996**, *323*, 757. For different applications of the method in exocytotic vesicular events see for example: b) D. J. Leszczyszyn, J. A. Jankowski, O. H. Viveros, E. J. Diliberto, Jr., J. A. Near, R. M. Wightman, *J. Biol. Chem.* **1990**, *265*, 14736; c) A. G. Ewing, T. G. Strein, Y. Y. Lau, *Acc. Chem. Res.* **1992**, *25*, 440; d) T. K. Chen, G. Luo, A. G. Ewing, *Anal. Chem.* **1994**, *66*, 3031; e) R. T. Kennedy, L. Huang, M. A. Atkinson, P. Dush, *Anal. Chem.* **1993**, *65*, 1882; f) E. H. Jaffe, A. Marty, A. Schulte, R. H. Chow, *J. Neurosci.* **1998**, *18*, 3548. For application to other biological events see for example: g) S. Arbault, P. Pantano, J. A. Jankowski, M. Vuillaume, C. Amatore, *Anal. Chem.* **1995**, *67*, 3382; h) S. Arbault, P. Pantano, N. Sojic, C. Amatore, M. Best-Belpomme, A. Sarasin, M. Vuillaume, *Carcinogenesis* **1997**, *18*, 569; i) S. Arbault, M. Edeas, S. Legrand-Poëls, N. Sojic, C. Amatore, J. Piette, M. Best-Belpomme, A. Lindenbaum, M. Vuillaume, *Biomed. Pharmacother. AIDS Sc. Sec.* **1997**, *51*, 430.

[7] E. Neher, A. Marty, *Proc. Natl. Acad. Sci. USA* **1982**, *79*, 6712.

[8] T. J. Schroeder, J. A. Jankowski, K. T. Kawagoe, R. M. Wightman, C. Lefrou, C. Amatore, *Anal. Chem.* **1992**, *64*, 3077.

[9] Under the conditions used in the experiments considered here,[5a–c] catecholamines are oxidized through an overall two-electron process; see: E. L. Ciolkowski, K. M. Maness, P. S. Cahill, R. M. Wightman, D. H. Evans, B. Fosset, C. Amatore, *Anal. Chem.* **1994**, *66*, 3611.

However, if the pH were lower and/or the time scale of diffusion shorter, a one-electron process might have to be considered instead, because the oxidation may stop at the level of the first cation radical intermediate since this has no time to deprotonate to yield the easily oxidizable phenoxy radical whose oxidation gives rise to the second electron exchange.

[10] a) J. Zimmerberg, M. Whitaker, *Nature* **1985**, *315*, 581; b) J. Zimmerberg, M. Cyrran, F. S. Cohen, M. Brodwick, *Proc. Natl. Acad. Sci. USA* **1987**, *84*, 1585; c) P. Verdugo, *Annu. Rev. Physiol*. **1990**, 52, 157.

[11] See, e.g.: a) D. J. Tanaka, D. J. Fillmore, *J. Chem. Phys.* **1979**, 70, 1214; b) however, this swelling is known to depend on the charge of the countercation for a polyanionic backbone, the gel being more compact the larger the positive charge. See e.g.: J. L. Barrat, J. F. Joanny, in *Advances in Chemical Physics, Vol. XCIV* (Eds.: I. Prigogine, S. Rice), Wiley, New York, **1966**, p. 1 ff.

[12] a) See e.g.: P. E. Marszalek, B. Farrell, P. Verdugo, J. M. Fernandez, *Biophys. J.* **1997**, *73*, 1160, and references therein; b) however, this swelling depends on the countercation, as established in ref. [11b]; see e.g.: P. E. Marszalek, B. Farrell, P. Verdugo, J. M. Fernandez, *Biophys. J.* **1997**, *73*, 1169.

[13] In the present case, adrenaline is a monocation and is presumably replaced by protons and other monovalent cations present in the extracellular medium. However, one must take into account that (although the exact structure of the polyelectrolyte complex is still unknown) the adrenaline cation is prone to form several strong hydrogen bonds to the carboxylate and other groups of the peptidic backbone, while the monovalent ions should only counterbalance the carboxylate charge and therefore give rise to dipole–dipole repulsion between the protonated or ion-paired carboxylate groups. Instead, exchange of the adrenaline cation by polycharged cations is expected to contract the matrix. This has indeed been reported for trivalent ions: for example, the lanthanum trication induces a measurable contraction of the matrix. See: M. J. Curran, M. S. Brodwick, *J. Gen. Physiol.* **1991**, *98*, 771.

[14] However, for other vesicles, the converse assumption is apparently retained by other authors; see ref. [12b], which examines the release of serotonin from secretory granules isolated from the beige mouse mast cell. Yet, from our point of view, their results[12b] only prove that i) swelling controls the diffusivity of serotonin, which can then be measured (ca. $10^{-8}\,cm^2\,s^{-1}$ depending on the extracellular medium composition), and that ii) the released flux correlates with the granule swelling. Nevertheless, neither of these facts disagrees with diffusion-controlled swelling and diffusion-controlled release as we advocate. Moreover, if the diffusivity of serotonin can be determined in their experiments, it means that diffusion of serotonin is the rate-determining step.

[15] A. J. Bard, L. R. Faulkner, *Electrochemical Methods*, Wiley, New York, **1980**.

[16] a) It is noted in Figure 5b, where the spike is merged with an evident foot component (left-hand column), that the normalized opened area function $\sigma(t)$ (middle column) presents an initial slope and that the correlation between simulated and experimental spike currents (right-hand column) shows two limiting linear components at short and long times, none of them with the expected slope of unity. This reflects the use of the convoluted diffusion equation [Eq. (8) and Brownian motion simulations] in the extraction procedure, although the pore release relates to a different kinetic situation. Thus, the extraction procedure compensates for the foot release; this leads to a smaller slope of I^{sim} vs. I^{exp} after the pore disappearance. The effect can be recognized and compensated for after a while, and used to eliminate the foot component. The effect is extremely sensitive, as observed in Figures 5a and 5c. Indeed, the experimental current spikes represented in these figures do not show an obvious foot component, but the same effect is observed in the corresponding correlations of I^{sim} vs. I^{exp}, albeit of lesser magnitude than in Figure 5b. Inspection of the ca. 600 spikes that have been treated show that ca. two thirds of the amperometric traces that do not show an obvious foot component (viz., $\simeq 70-80\,\%$ of the events) present this characteristic feature of a foot release merged with the rising part of the spike release. Since this indicates that the foot release occurred for $\simeq 0.5-1$ ms for these events, this validates a posteriori our evaluation of an average of ca. 2 ms duration for a foot release under our conditions. b) In this context, it is interesting to note that under our conditions, the foot release occurs over an average time less than that observed in patch-clamp experiments. This may result from the fact that the electrode screens the diffusion of divalent ions used for eliciting the exocytotic behavior (Ba^{2+} under our conditions) to the pore entrance, so that in the vesicle matrix, exchange of the adrenaline cation should occur mainly by monovalent ions [note that Eq. (1) indicates that two protons are produced in the artificial synaptic gap per adrenaline cation detected]. Since the alteration energy per exchanged site in the matrix is expected to be larger when the exchange involves monovalent ions rather than divalent ones (see refs. [12b, 13]), the fact that we observe shorter foot releases than in patch-clamp experiments is perfectly consistent with our considerations on the transition between foot and spike release.

[17] C. Amatore, Y. Bouret, E. R. Travis, R. M. Wightman, unpublished results.

[18] J. P. Dadoune, in *Histologie*, Flammarion Médecine-Sciences, Paris, **1990**, pp. 174–176.

[19] a) T. G. Strein, A. G. Ewing, *Anal. Chem*. **1992**, *64*, 1368; b) T. J. Schroeder, J. A. Jankowski, J. Senyshyn, R. W. Holz, R. M. Wightman, *J. Biol. Chem.* **1994**, *269*, 17215.

[20] C. Amatore, J. M. Savéant, *J. Electroanal. Chem.* **1977**, *85*, 27.

Received: November 16, 1998 [F1449]

 © WILEY-VCH Verlag GmbH, D-69451 Weinheim, 1999 0947-6539/99/0507-2162 $ 17.50+.50/0